Design, Analysis and Hover Performance of a Rotary Wing Micro Air Vehicle

Felipe Bohorquez, Paul Samuel, Jayant Sirohi, Darryll Pines, Lael Rudd
Smart Structures Laboratory, Alfred Gessow Rotorcraft Center
Department of Aerospace Engineering, University of Maryland
College Park, MD 20742

Ron Perel
Johns Hopkins University/Applied Physics Laboratory
Laurel, MD 20725

An initial design concept for a micro-coaxial rotorcraft using custom manufacturing techniques and commercial off-the-shelf components is discussed. Issues associated with the feasibility of achieving hover and fully functional flight control at small scale for a coaxial rotor configuration are addressed. Results from this initial feasibility study suggest that it is possible to develop a small scale coaxial rotorcraft weighing approximately 100 gm, and that moment control is sufficient for roll, yaw and lateral trim. A prototype vehicle was built and its rotors were tested in a custom hover stand used to measure thrust and power. The best measured rotor Figure of Merit, 0.42, was obtained for a single rotor configuration. A blade element momentum theory (BEMT) model of the rotor was implemented, and airfoil characteristics were estimated from the rotor tests. The model showed that profile drag accounts for 45% of the losses as opposed to 30% in full-scale helicopters. The radio controlled vehicle was flown untethered with its own onboard power source and exhibited good flight stability and control dynamics.

Nomenclature

A_f	flap area
A_g	reference area
A_r	rotor disk area
C_D	sectional drag coefficient
C_{D0}	zero lift drag coefficient
C_{Df}	sectional flap drag coefficient
$C_{l\alpha}$	lift-curve slope
$C_{l\alpha f}$	flap lift-curve slope
C_P	power coefficient
C_{P0}	profile power coefficient
C_{Pi}	induced power coefficient
C_T	thrust coefficient
d_f	flap moment arm
d_g	gust moment arm
d_T	thrust moment arm
F_f	flap force
M_f	vechicle roll/pitching moment produced by flap deflection
M_g	moment acting on a cylinder in a gust
M_T	vechicle roll/pitching moment produced by thrust deflection
n	blade element number
r_n	radius of blade element n
T	rotor thrust
V	local wind velocity perceived by flap
V_g	gust velocity
α	blade section angle of attack
α_f	flap angle of attack
θ	blade pitch angle
θ_T	deflection of thrust vector
θ_{75}	pitch angle at 75% radius
κ	induced power factor
λ	rotor inflow ratio
ρ	air density
σ	rotor solidity

Abbreviations

BEMT	blade element momentum theory
FM	figure of merit
IGE	in-ground effect
MAV	micro air vehicle
MICOR	micro coaxial rotorcraft
RPM	revolutions per minute

Introduction

Recent advances in electrical and mechanical system miniaturization have spurred interest in finding new solutions to an array of military and civilian missions. One such solution is the Micro Air Vehicle (MAV) (Refs. 1, 2). These vehicles are an order of magnitude smaller than previously developed systems and operate in a low Reynolds number aerodynamic regime (Fig. 1). Due to their unique capabilities, MAVs are applicable to such missions as covert imaging, biological and chemical agent detection, battlefield surveillance, traffic monitoring, and urban intelligence gathering. Rotary wing vehicles have significant advantages over fixed wing vehicles for these types of missions, particularly when the vehicle is required to remain stationary (hover) or maneuver in tightly constrained environments. For example, intelligence gathering around or within buildings requires a hovering vehicle with good maneuverability characteristics. It is important to point out that hover is an intrinsically high-power flight state and energy consumption will be a primary consideration. It is expected that recent advances in both battery and novel power supply technology (e.g. fuel cell) will allow reasonable endurance to be achieved without sacrificing hover capability. Hovering vehicle cofigurations include conventional rotorcraft, ducted fans, and coaxial rotors.

This paper presents an initial design and analysis of a prototype rotary wing MAV called MICOR (MIcro-COaxial Rotorcraft). MICOR has been designed to exploit the advantages of rotary wing flight and is expected

Manuscript received July 2001; accepted January 2003.

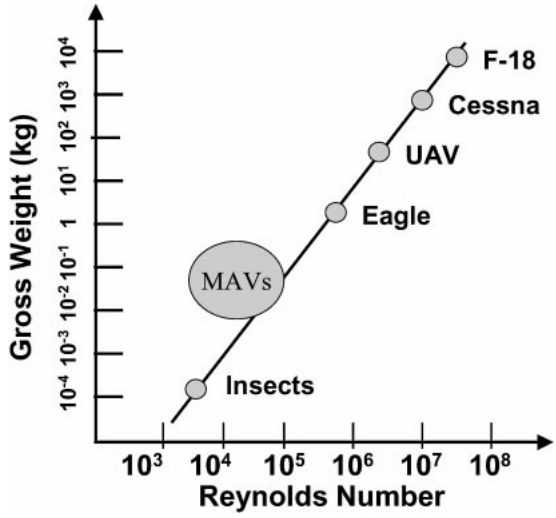

Fig. 1. Relative magnitudes of various aircraft.

to be best suited to missions where hover performance is desired. The optimal mission would require that the vehicle be delivered close to the point of interest. The vehicle would then be able to investigate the target, e.g. fly through a building or hold position outside a window, while sending information back to the operator.

Design Requirements

To establish performance and design requirements, the decision was made to conform to the definitions employed by the DARPA MAV program initiated in 1996 (Ref. 3). Thus, the overall dimensions of the MAV were restricted to less than 6 inches (15.24 cm) in length, width or height. A gross takeoff weight of approximately 100 gm was set as the target weight for the MAV design. A specific sensor was not selected, however the payload weight was chosen to be nominally 10 gm, which is enough to carry a miniature color camera and its transmitter.

In addition, it was decided that the baseline MAV design would be restricted to a rotary wing configuration. Hence, the vehicle was required to have good hover performance over an altitude of 100 meters. Extended range requirements were not set for the MAV design since efficient forward flight is not a strength of a rotary-wing configuration. It was anticipated that, in a situation where the target is far from the point of origin, an external delivery method (e.g. a mothership UAV or large scale munition) might be employed to transport the MAV. In order to facilitate delivery, the vehicle must be compactly packaged and able to withstand high g-loading.

When a specific mission requires the surveillance of a target from a fixed location, the ability to perform multiple landings and takeoffs during a single mission becomes important. After reaching the target the vehicle could land without interrupting data transfer, saving energy and thus increasing the systems versatility and potential mission duration. For example the mission scenario, shown in Fig. 2, is to take surveillance imagery through building windows from nearby rooftops and to monitor traffic flow. If the target moves, the vehicle could take off and relocate to a new position. Finally, the MAV design should fulfill these requirements with a minimum of mechanical complexity. Table 1 summarizes some additional requirements[1] for the baseline MAV considered in this study.

[1]Commercially available micro helicopters (i.e. Schweizer Hornet, Ikarus Piccolo, MIA Robin 280) have rotor diameters between 20 and 50 cm and weights between 0.5 and 1.3 kg. They can fly for less than 10 min and have minimal payload capabilities.

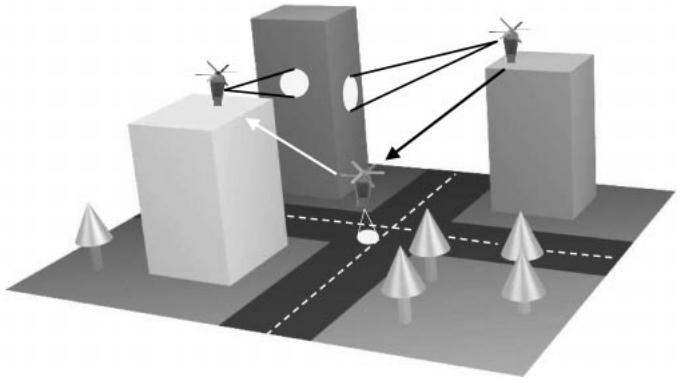

Fig. 2. MAV urban mission scenario.

Table 1. Baseline MAV design requirements

Desired hover time	20 to 30 min
Payload weight	10 gm
Gross takeoff weight	100 gm
Altitude	100 m
Size	$\leq$15.24 cm
Desired cruise speed	10–20 km/h
Desired range	5 km
Gusts\crosswind	5 m/s
Navigation	Line of sight tracking from ground

Concept Selection

In order to select a configuration for the vehicle, different concepts were systematically compared. Selection was made based on the criteria listed below:

1) Hover efficiency
2) Compactness of stored/transported vehicle
3) Ease of payload packaging
4) Simplicity of structure
5) Controllability
6) Maneuvrability
7) Environmental friendliness and noise

Configurations considered

The configurations considered can be broken into four categories: single rotor, twin rotor, quad rotor, and hybrid helicopter.

Single rotor configurations. These are conventional main rotor/tail rotor, rotors with vanes in the slipstream for providing anti-torque (Ref. 4), and tip-jet driven rotors (Ref. 5). The first two of these configurations have been successfully tested for UAVs and MAVs (Refs. 4, 6). The conventional main rotor/tail rotor design provides good aerodynamic efficiency and has good controllability and maneuvrability. However, compactness in folding is adversely affected by the tail boom and, comparatively, a large size of the rotor is required. The tail rotor drive system introduces additional mechanical complexity and power requirements that can be avoided using other designs. Vanes in the wake of the rotor working as antitorque devices add weight and make the vehicle larger and harder to fold/store. Finally, tip-jets are attractive for their simplicity and ease of payload packaging as a result of the absence of a powerplant inside the fuselage. However, they have the drawback of poor controllability which

may be attributed to the high blade inertia resulting from blade mounted nacelles.

Twin rotor configurations. Four twin rotor configurations were considered: coaxials, side-by-side rotors, tandems and ducted coaxial configurations. The coaxial design is favored by most of the key design criteria: compactness of folding, simplicity of structure and ease of packaging. Side-by-side and tandem configurations have similar characteristics. Their hover efficiency is higher than that of the coaxial configuration. However, the difficulty of folding and the complexity of the structure and transmission are among the key drawbacks of side-by-side and tandem configurations. Ducted coaxial designs are well suited for MAVs, but have significant compactness problems since shrouds and ducts cannot be stored efficiently. A ducted coaxial configuration has been widely used for UAV design, for which Sikorsky's Cypher and Cypher II are good examples (Ref. 7).

Quad rotor and other rotor configurations. Recently, there has been an interest in the rotorcraft industry in designing rotorcraft with four or more lifting rotors. Such configurations could be controlled by varying the RPM of different rotors to change the direction of the thrust vector. Some small scale examples include the Mesicopter (Ref. 8), the Gyronsaucer and the Roswell Flyer. The last two are commercially available RC helicopters and are reported to have very good controllability. The Mesicopter, a meso-scale flying machine which is no larger than a penny, is still in the development stage. A quad rotor design can have good hover efficiency as well as good handling and control characteristics, however packaging complexity is again an important drawback.

Hybrid helicopter configurations. The candidates in the compound helicopter category are rotor wing or stopped rotor, tilt-rotor, tilt-wing, joined wing, and toroid rotor configurations (Ref. 9). All these designs prove difficult to achieve a compact stored/transported state because of the large size of their lifting surfaces. They are all well suited for payload packaging and also very effective in high-speed forward flight. However, as the design requirements do not include high speed forward flight, these configurations are not suitable options.

From this qualitative assessment it can be concluded that the conventional single rotor/tail rotor configuration, the quad rotor and the coaxial design, are the best candidates for the present design problem. The coaxial configuration has the advantages of compactness of folding and ease of deployment while the quad rotor is superior from a controllability view point. However, given the relative strength of the compactness requirement, the folding problems associated with the quad rotor preclude its use. Hence, the final configuration chosen is that of a coaxial rotorcraft.

Vehicle configuration

The prototype vehicle, displayed in Fig. 3, has a coaxial rotor configuration with an axisymmetric fuselage. As mentioned before, the coaxial configuration is employed since it is compact and provides inherent anti-torque capability. Because of this anti-torque capability, a tail rotor supported by a tail boom is not needed for yaw stabilization, and thus all power can be devoted to useful vertical lift. Additionally, in an attempt to simplify the mechanical design, the swashplate is eliminated and the blades are rigidly attached to the hub (no hinges or bearings).

Because the system has no swashplate or tail rotor, a nontraditional control scheme has to be employed for the roll, pitch and yaw axes. Each rotor is driven by a separate motor which allows yaw control to be performed by varying the difference in rotational speed between the two rotors. This changes the torque transmitted to the fuselage. For control of vertical velocity, total thrust is adjusted by varying the motors' rotational speeds simultaneously.

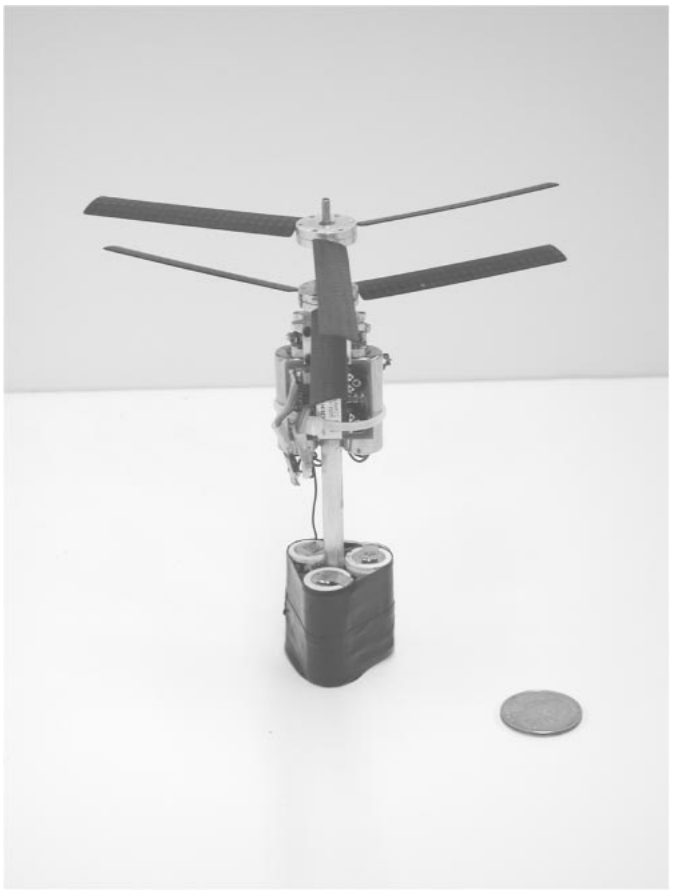

Fig. 3. MICOR prototype.

Different lateral control methods were considered for MICOR: aerodynamic flaps or fins to deflect the downwash of the rotors, a gimballed drivetrain/rotor for thrust vectoring, and ducted fan and/or reaction jets to impose rolling and pitch moments. The selection of any of these methods will influence the configuration of the vehicle. Control issues are discussed in detail in a later section.

Vehicle Design

The prototype Micro Coaxial Rotorcraft (MICOR) vehicle was conceived to meet the design requirements in the least complex manner. Hence, commercial off-the-shelf components were used whenever possible. However, many components were custom designed and fabricated prior to assembly.

Propulsion

With the baseline design requirements previously mentioned, a minimum total thrust (produced by the two rotors) of 100 gm is needed to hover. Assuming a rotational speed of 4,500 RPM and a conservative Figure of Merit of 0.5 for a small scaled rotor, the required baseline shaft power for hover for each rotor is 3 W. If an electric motor-transmission system is chosen with a 65% efficiency, the baseline electrical power required is approximately 4.5 W. Because of the separation between the two rotors, theory states that for a fully developed upper rotor wake, half

Table 2. Motor performance comparison

Parameter	WES-Technik[a] DC 6-8.5	WES-Technik DC 5-2.4	MicroMo DC 1717
Rated voltage (V)	6	5	3
No load speed (rpm)	25,200	21,000	12,600
Stall torque (gm-cm)	131	44.8	39.7
Maximum output power (W)	8.52	2.42	1.41
Maximum efficiency (%)	77.3	75.3	66
Weight (gm)	17	10	17

[a]Motor chosen for MICOR.

the area of the lower rotor operates in an effective climb velocity. As a result, the induced power is increased by a factor of approximately 1.28 times (Ref. 10) the induced power of two independent rotors producing the same thrust. Assuming that the power consumed is 70% induced and 30% profile, the total power required for hover is 10.8 W. To ascend and maneuver, at least an extra 30% of this power is needed. Thus, 15 W of available power was set as a design requirement.

To produce this power, a variety of options are available including electric motors, internal-combustion engines, turbines, thermopiles, chemomechanical engines, remote powering methods, fuel cells and compressed gas (Ref. 11). Of these power/propulsion options, fuel cell technology and new flexible lithium batteries appeared to be the most promising for future MAVs. However, few, if any of these systems have been built for small scale vehicles. The most readily available clean and efficient propulsion option is battery driven electric propulsion.

The batteries selected for the MICOR are three 3-V lithium $LiMnO_2$ cells, each with a capacity of 430 mAh. Assuming an average power consumption of 13 W and a constant operating voltage of 9-V, the current drain of the system is 1.45 A. If the batteries are capable of providing this constant current flow, then the MICOR would fly for 17 minutes. However, the discharge rate required is too large, and it is unlikely that the batteries can maintain the required current flow for a long time. Nevertheless, because of their large energy density lithium cells were chosen in this initial design study. The electric motor chosen for the MICOR configuration was a commercial off-the-shelf 6-V coreless DC motor. This motor was chosen for its high power output as compared to other electric motors of similar size and weight (see Table 2).

Rotor blades and hub

Curved plate airfoils have relatively good aerodynamic performance at low Reynolds numbers (Refs. 12, 13), plus they are easy to manufacture. Hence, a thin curved plate airfoil with 8% constant radius camber was chosen. Each blade has a chord of 1 cm and a length of 7 cm (constrained by the overall vehicle size requirement). The solidity ratio of each three bladed rotor is 0.119, with a root cut-out of 1 cm, and a coning angle of 0 deg. The blades consist of three layers of graphite/epoxy weave prepreg with a layup of (+45, 0, +45). To manufacture the blades, a simple mold composed of a top concave surface, a bottom convex surface, and an edge dam was machined from aluminum.

The composite was placed in the mold, clamped and cured. The resulting blades are very consistent and require only minimal post cure processing. Finally, a small aluminum pin was bonded to the root of the blade. The root pin has a flat surface along a portion of its length to aid in bonding, and the opposite end is flared to transfer axial loads from the blades to the hub.

The rotor hub consists of two parts, top and bottom, that clamp onto the root pin, constrain its rotation, and thus fix the collective pitch of the blades. A space was left in the hub for the flared end of the root pin. This design allows the blade collective pitch to be changed between tests.

Fig. 4. MICOR transmission configuration.

The upper and lower rotor hubs are screwed onto external threads on the coaxial shafts; this design allows one to easily modify the spacing between rotors. A rotor spacing of 1 in (0.35 R) was chosen after some preliminary testing. Experimental results showed a small influence of this parameter on the vehicle performance. These results are similar to those presented in Ref. 14.

System integration

The vehicle configuration requires that each rotor be driven by a separate motor. However, the rotors are coaxial while the motors are not. The motors are mounted parallel to the axis of rotation of the rotor shafts. Each motor/rotor system consists of a pinion mounted to the motor shaft that in turn drives a gear attached to the rotor shaft. In order to let the shaft axis of rotation for each rotor be coaxial, the gears, and thus the pinions, must be offset vertically. Since the motors are not coaxial, the pinions must also be offset horizontally with each pinion being coaxial with its corresponding motor. The transmission housing was designed to support the gears, rotor shafts and motors, and transmit the rotor loads from the rotor system to the rest of the structure. The primary structural member is a thin walled shaft mounted to the bottom of the transmission housing. This shaft gives support for the motors, batteries, electronics and payload. The resulting configuration is shown in Fig. 4. The final transmission design consists of an 8 tooth pinion and a 30 tooth gear resulting in a reduction ratio of 3.75:1. In addition to having the desired reduction ratio, this configuration provides enough space between the motors for the structural shaft. A weight breakdown of the vehicle is shown in Table 3.

Table 3. MICOR's weight breakdown

Component	Weight Percentage
Motors & transmission	40%
Batteries	30%
Structure	12%
Electronics	9%
Payload	9%

Flight Control

A fully functional flight control system is an absolute necessity for MICOR. A typical rotorcraft control system (swashplate, pitch links, etc.) is quite complex; this is especially true for a coaxial rotor configuration. This complexity is prohibitive for MICOR as it would significantly increase the vehicle's weight and hub drag. To simplify the mechanical design, the swashplate is eliminated and the rotor blades are rigidly attached to the hubs. Hence, a nontraditional flight control system must be developed.

Yaw and thrust control

Yaw control and thrust (altitude) control can be accomplished by varying the RPM of the rotors. Yaw control can be performed by varying the difference in rotational speed between the two rotors, creating a torque applied to the fuselage. Thrust is adjusted by varying the rotors' RPMs equally.

Lateral control

Two lateral control methods were considered for MICOR: aerodynamic surfaces (flaps) and gimballed drivetrain/rotor for thrust vectoring. The systems were considered from the standpoints of mechanical complexity, control algorithm complexity, and power required. These control systems are shown in Figs. 5 and 6, respectively.

Of the two systems, the aerodynamic flap system would be the easiest to implement and would require only a small amount of power to operate. A more traditional control scheme would be to use fins that are mounted perpendicular against the fuselage, embedded in the rotor downwash. However, flap control was chosen over fin control for two reasons. First, the flap system is more compact since, except during maneuvers, the flaps remain flush to the fuselage. Second, flaps can be easily located at a radial position with larger downwash velocities, increasing the available control moments. Flaps can also provide support as landing gear for the vehicle when it is at rest on the ground. One disadvantage of the flap control scheme is the possible loss of effectiveness in a gust or crosswind and at relatively large forward flight speeds. Development of stability and control algorithms using this control method was determined to be a tractable problem.

The gimballed rotor/motor system, though slightly more complex than the aerodynamic flap system, ultimately yields the cleanest aerodynamic vehicle configuration, and potentially requires the least amount of power to operate. Once again, the development of stability and control algorithms using this control method was determined to be a tractable problem.

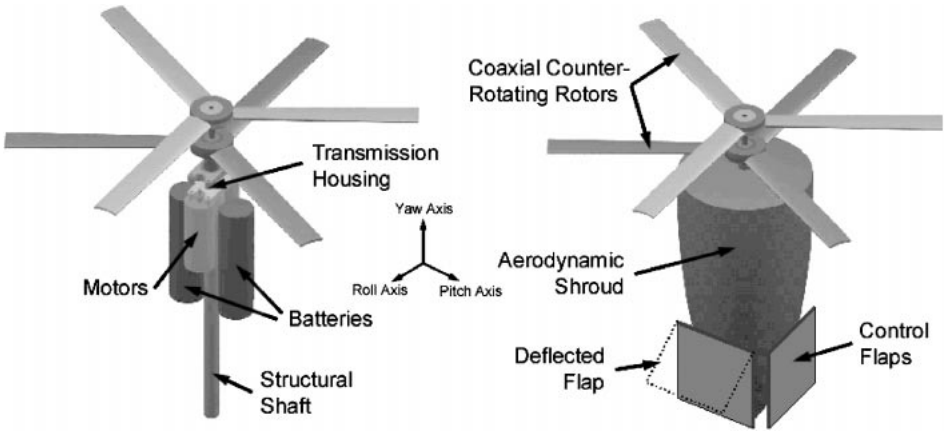

Fig. 5. Aerodynamic flaps.

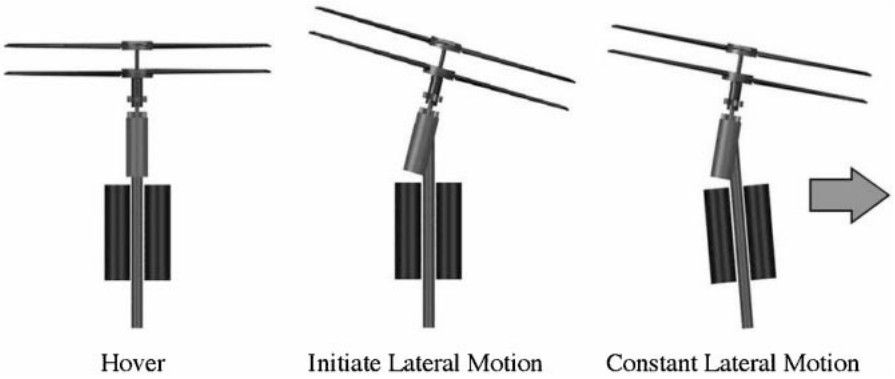

Fig. 6. Gimballed drivetrain/rotor.

Available control moments

Two of the lateral control systems mentioned previously have been studied for MICOR: aerodynamic flaps and a gimballed drivetrain/rotor (hinged mass). First, the pitch/roll moments each configuration can generate are estimated for a general vehicle, then values for disturbance moments generated by gusts are estimated. In the hinged mass configuration, the plane of the rotor system is tilted with the use of servos, thus reorienting the thrust vector and causing body moments. In the aerodynamic flap configuration, moments are generated by deflecting flaps into the rotor downwash.

The following analysis predicts the magnitude of the moments that each system can generate, and then discusses whether or not we expect these moments to translate to sufficient bandwidth for a coaxial rotorcraft in a noisy environment. All the analysis is performed for the simplified case of the vehicle in hover.

The moment generated by a deflection of the thrust vector by Θ_T degrees and moment arm d_T is

$$M_T = d_T T \sin\Theta_T \tag{1}$$

Typical values for MICOR are easily found. Thrust, T, equals the weight of the system, approximately 1 N. To maximize available moments in this configuration, the heaviest components would be placed near the bottom of the vehicle to maximize d_T. It is assumed that a d_T of 10 cm is achievable. Lastly, a typical value must be chosen for Θ_T. Considering that for practical purposes the vertical component of thrust is not wanted to change by more than a few percent, a generous upper bound for Θ_T is 15 deg. Therefore, substituting in these values, the maximum expected moment is

$$M_T = .026\ \mathrm{N}\cdot\mathrm{m} \tag{2}$$

For the aerodynamic flap configuration, the moment generated by a flap force F_f is simply $d_f F_f$ where d_f is the effective moment arm. If it is assumed that the flaps have a constant lift curve slope of $C_{l\alpha f}$, then the moment for a flap deflection of α_f becomes $\frac{1}{2} d_f C_{l\alpha f} \alpha_f \rho V^2 A_f$, where V is the local wind velocity and A_f is the surface area of the flap. If it is further assumed that the flaps operate in the fully contracted rotor downwash, then from simple momentum theory V becomes $\sqrt{2T/\rho A_r}$, where ρ is the air density and A_r is the surface area of the rotor disk. Therefore, the total moment due to the flaps can be written

$$M_f = \frac{T A_f d_f C_{l\alpha f} \alpha_f}{A_r} \tag{3}$$

For this configuration, the center of gravity of the vehicle should be placed as close to the rotors as possible, and place the flaps far from the rotors. With this strategy a d_f of 10 cm should be achievable. Given a typical rotor diameter of 15 cm, air density at sea level of 1.225 kg/m^3, flap surface area of 50 cm^2, conservative lift curve slope of π per radian and a maximum flap deflection of 30 deg, the expected maximum moment due to flaps at hover is

$$M_f = 0.017\ \mathrm{N}\cdot\mathrm{m} \tag{4}$$

The typical fin surface area of 50 cm^2 is calculated by assuming two fins of surface area 25 cm^2 on either side of the fuselage and deflecting in the same direction. If the flaps are mounted flat against the fuselage such that only one could be deflected, the available moments produced by the lift force are cut in half, and an additional moment produced by the drag force on the flap has to be included in the analysis.

Considering the simplified nature of moment approximations, the one-third greater estimated moment of the flap configuration is somewhat negligible. The interesting result is that each configuration produces moments of approximately the same magnitude at around a few hundredths of a Newton · meter. A more detailed analysis would consider numerous additional factors, including better approximations of the rotor downwash velocity and available flap forces. In practice, it is easier to move the center of gravity closer to the rotor than further away since the transmission and motors must necessarily be located near the rotor. This tends to favor the aerodynamic flap configuration.

Now that the approximate magnitudes of the available moments are known, the next logical step is to determine if these moments are large enough to attenuate the disturbance moments acting on MICOR. The primary disturbance source is wind gust. Because the vehicle is so small and dense, disturbances are relatively small. An approximation of the order of magnitude of gust disturbances can be generated by modelling MICOR as a cylinder. The moment acting on a cylinder in a gust can be written as

$$M_g = \frac{1}{2} C_{Df} \rho V_g^2 A_g d_g \tag{5}$$

where C_{Df} is the flap drag coefficient, ρ is the air density, V_g is the gust velocity, A_g is the reference area and d_g is the moment arm. For MICOR, $C_{Df} = 1$, $\rho = 1.225$ kg/m^3, $A_g = 0.003$ m^2 and $d_g = 0.05$ m (based on the actual vehicle dimensions). Using these values and a large gust velocity of 5 m/s yields a gust moment of 0.0023 N · m, which is an order of magnitude lower than the achievable command moments.

Hover Performance

While the hover performance of more conventional full-scale rotorcraft configurations is well documented in the literature, the hover performance of micro air vehicles in hover at low Reynolds numbers is relatively unknown (Ref. 15). Thus, the baseline MICOR vehicle was flown in a laboratory environment, and its rotors were tested in a custom designed hover stand to evaluate its performance.

Mathematical models

In estimating the efficiency of low Reynolds number rotors in hovering flight, it is important to consider losses that affect hover performance including induced and profile drag, nonuniform inflow, slip stream rotation, and tip losses. Comparing the actual power required to hover with the ideal power required to hover leads to the rotor Figure of Merit, *FM*, given by

$$FM = \frac{ideal\ hover\ power}{actual\ hover\ power} = \frac{C_T^{3/2}}{C_P\sqrt{2}} \tag{6}$$

where C_T and C_P are the thrust and power coefficients, respectively. The *FM* can be used as a measure of the efficiency of a rotor generating thrust for a given power. However it should only be used as a comparative measure between two rotors at the same blade loading.

While simple momentum theory can be used as a first approximation to estimate the efficiency of rotors, a more accurate aerodynamic theory is needed to incorporate blade geometry, sectional orientation and twist condition. Blade element theory evolved to incorporate the effects of drag and twist on rotor performance. This theory permits the derivation of the following equations for the thrust and torque coefficients:

$$C_T = \frac{1}{2}\sigma C_{l\alpha}\left(\frac{\theta_{75}}{3} - \frac{\lambda}{2}\right) \tag{7}$$

$$C_P = \kappa\frac{C_T^{3/2}}{\sqrt{2}} + \frac{C_{D0}\sigma}{8} \tag{8}$$

where θ_{75} is the blade pitch angle taken at 3/4 radius, λ the rotor inflow ratio, C_{D0} is the zero lift drag coefficient and σ is the rotor solidity. In order to include the nonideal aerodynamic effects such as nonuniform inflow, tip losses and wake swirl, the coefficient κ known as the induced power factor is included in the induced power expression. Substituting Eq. (8) into Eq. (6) leads to the following expression of *FM*:

$$FM = \frac{\frac{C_T^{3/2}}{\sqrt{2}}}{\kappa \frac{C_T^{3/2}}{\sqrt{2}} + \frac{\sigma C_{D0}}{8}} \tag{9}$$

The blade element momentum theory (BEMT) is a method that combines the momentum and blade element theories and allows one to estimate the inflow distribution along the blade. It is a common practice to solve the BEMT equations numerically by discretizing the blades into a series of small elements. The rotor inflow ratio at each n element, $\lambda(r_n)$, is given in the numerical implementation of the BEMT in hovering conditions by

$$\lambda(r_n) = \frac{\sigma C_{l\alpha}}{16}\left[\sqrt{1 + \frac{32}{\sigma C_{l\alpha}}\theta(r_n) r_n} - 1\right] \tag{10}$$

where r_n and $\theta(r_n)$ are the radius and the pitch angle at the midspan of each of the n elements, respectively. Equation (10) allows one to solve for the inflow as a function of the radius for any given airfoil section and blade geometry. After the inflow is determined, the incremental thrust of each blade element is obtained using

$$\Delta C_T = \frac{\sigma C_{l\alpha}}{2}(\theta(r_n) r_n^2 - \lambda(r_n) r_n)\Delta r \tag{11}$$

The total thrust is calculated by numerically integrating over the blade. The induced power coefficient, C_{Pi}, and profile power coefficients, C_{P0}, are also calculated numerically using the following equations:

$$C_{Pi} = \int_{r=0}^{r=1} \lambda \, dC_T \tag{12}$$

$$C_{P0} = \frac{\sigma}{2}\int_{r=0}^{r=1} C_D(r) r^3 dr \tag{13}$$

The induced power factor is found using Eq. (14) after solving Eq. (12) to find the induced power coefficient and numerically integrating Eq. (11) along the blade span to calculate the rotor thrust coefficient C_T. That is,

$$\kappa = \frac{C_{Pi}}{C_T^{\frac{3}{2}}/\sqrt{2}} \tag{14}$$

The *FM* can be determined by using Eq. (6) with the numerically calculated induced power, power factor and the profile power.

Experimental setup

In order to determine the performance of MICOR's rotors for a range of thrust coefficients, a hover test stand was designed and built. The test stand, shown in Fig. 7, is an instrumented platform where the MAV's motor-transmission system is mounted with one or two rotors via a stem. The rotors are inverted so that the air flow goes from bottom to top. This avoids In-Ground Effect (IGE) thrust influence on rotor performance,

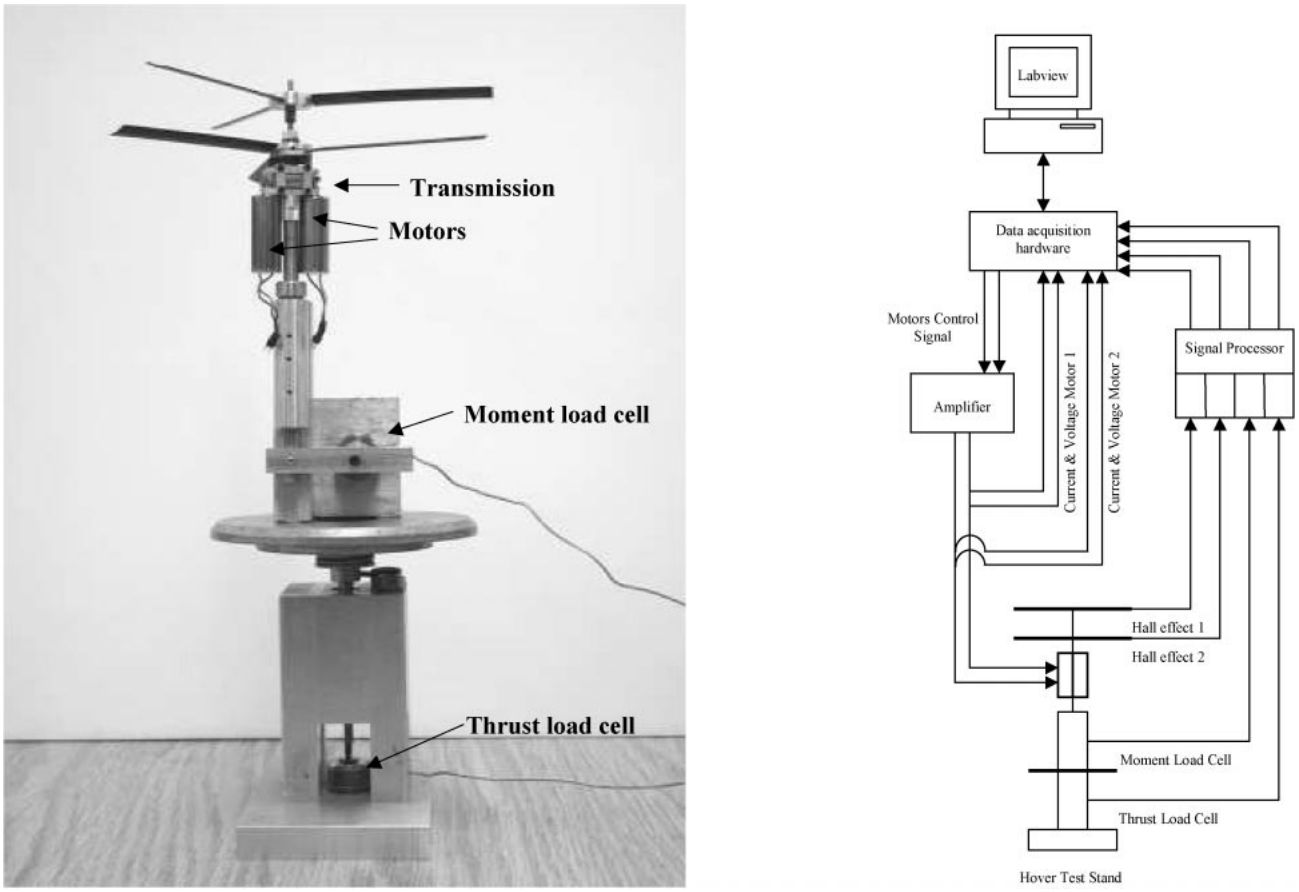

Fig. 7. Experimental setup (a) hover stand and (b) schematic of data acquisition system.

Table 4. Coaxial tests results

	15-15 Collective Pitch			15-18 Collective Pitch			18-18 Collective Pitch		
	RPM	P_{elec} (W)	Thrust (gm)	RPM	P_{elec} (W)	Thrust (gm)	RPM	P_{elec} (W)	Thrust (gm)
Upper rotor	4,517	8.1		4,249	8.1		4,000	8.17	
Lower rotor	4,548	7.8		3,930	7.8		4,041	8.23	
Total		15.9	110.26		15.9	112.57		16.5	110.15

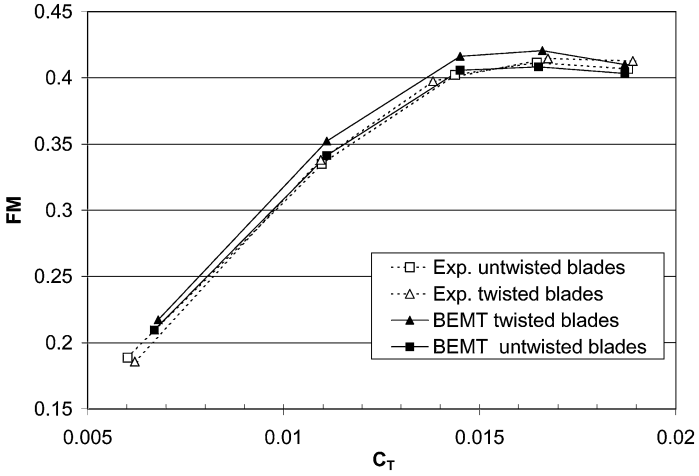

Fig. 8. Figure of merit vs. C_T, twisted and untwisted blades, experimental and BEMT results.

and simplifies the thrust measurement (directed downwards on the load cell arrangement).

Thrust and moment are measured using two load cells. The transmission's support can rotate freely, and moment is transmitted to a load cell by a 1 in arm. Thrust is measured by the second load cell placed directly under the platform's shaft. Each rotor's rotational speed is determined using a Hall effect sensor. Additionally, the voltage and current supplied to the motors are also measured to obtain the electrical power consumption. All the data was acquired and processed by a data acquisition system linked to a computer running LabView.

Experimental results

Two main sets of experiments were performed: (a) single rotor tests with twisted (-10 deg linear twist) and untwisted blades and, (b) coaxial configuration tests using only untwisted blades. For the single rotor tests the collective pitch was increased from 6 to 18 deg in steps of 3 deg. In the coaxial configuration tests, three collective pitch settings were tested: 15 deg upper and lower rotors, 18 deg upper and lower rotors, and 15 and 18 deg upper and lower rotors, respectively.

Single rotor tests. For every collective pitch, rotational speeds were varied between 3,000 and 4,500 RPM. In general for each collective pitch tested, *FM* had small variations with a tendency to increase at higher rotational speeds. In Fig. 8 only these maximum values are plotted, and the results for twisted and untwisted blades are compared. Notice that the *FM* curves are similar to full-scale rotors as a general trend, though not in overall magnitude. The use of twist in the rotor blades gives a more uniform inflow, and at high Reynolds numbers, Re, this reduces primarily the induced power. In a full-scale helicopter a large increase in *FM*, up to 10%, can be obtained. However, experimental results show that only approximately 2% increase in *FM* for the higher thrust coefficients is gained by twisting the blades.

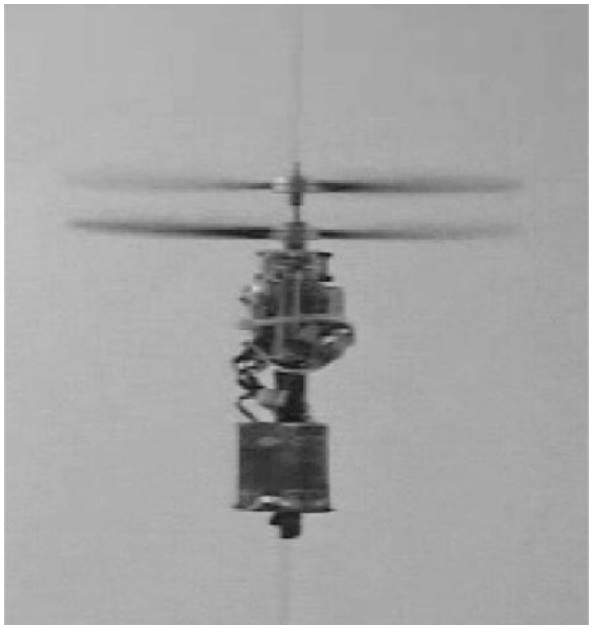

Fig. 9. MICOR in untethered hovering flight.

Coaxial configuration tests. The purpose of this set of tests was to determine the best collective pitch setting of the two rotors to allow the current prototype carrying a 10 gm sensor to hover. Total thrust and each rotor's rotational speed were measured. The current supplied to the upper rotor was fixed, while the current given to the lower rotor was set such that there was no net torque applied to the fuselage. Mechanical power was not measured and only electrical power consumption, *Pelec*, was used for comparisons. The results are shown in Table 4.

For the different collective pitch settings tested, relatively small differences were found. The collective pitch combination that provided the largest thrust to power ratio was the 15 deg upper rotor and 18 deg lower rotor. Due to the wake of the upper rotor, the lower rotor has a reduced effective angle of attack, so it is convenient to set its collective pitch higher than the optimal. The total power consumption was similar to that of the $15-15$ deg case, however 2 extra gm of thrust were produced. The $18-18$ arrangement gave similar thrust values than the $15-15$ arrangement, but with higher power requirements.

Finally, the rotors tested in the coaxial configuration at $15-15$ deg pitch angle of attack yielded a measured thrust capability of 110 gm. This is approximately 5% less than twice the value obtained with a single rotor at the same rotational speed.

Test flights. The prototype had an overall takeoff weight (without sensor) of 100 gm, 10 more grams than the baseline requirement. The batteries account for 30% of the total weight, making them the heaviest component of the vehicle. Since lateral control was not implemented, the prototype was tested in vertical flight using a nylon string for guidance (Fig. 9). The efficiency of the motors-transmission system was defined as the ratio

between the output mechanical power and the input electrical power; it was found to be 60% with small variations for the different testing conditions. This value is 5% lower than the initial estimate. As expected the large current draw of the system considerably reduced the performance of the batteries, leading to hover times of only 3 min instead of the 17 min initially predicted.

During the test flights, the MICOR prototype demonstrated acceptable stability characteristics with a slight tendency to roll. However, with the implementation of a closed loop lateral control system this difficulty can be overcome. Open loop altitude and yaw control were satisfactorily achieved.

Discussion

For the single rotor tests, the highest Figure of Merit values ($FM = 0.42$) were obtained at 4,500 RPM and 15 deg collective pitch, which corresponds to a C_T of 0.0165. Thrust values of 60 gm were measured with an electric power consumption of 8 W. This was chosen as the hover operating point of the vehicle since it is close to the design requirements.

The rotor's tip Re is around 25,000 (at 4,500 RPM). For such a low Reynolds number there is a degree of uncertainty in the value of the zero lift drag coefficient, C_{D0}, and in the induced power factor, κ. Experimental studies suggest that C_{D0} at low Re for conventional NACA series airfoils may range from 0.05 to 0.0084 at $\mathrm{Re} = 1 \times 10^4$ and 3×10^5, respectively, and for curved plates may range from 0.17 to 0.08 at $\mathrm{Re} = 1 \times 10^4$ and 6×10^4, respectively (Refs. 12, 13, 16, 17). The actual value depends on the viscous drag effects, geometry and surface roughness of the manufactured airfoils.

Assuming a constant value for the induced power factor, the zero lift profile drag coefficient can be calculated using the measured power coefficients and Eq. (8). This is a very rough approximation that does not take into account the variation of κ for the different thrust coefficients.

A more accurate approach to determine the contributions of the profile and induced losses to the power coefficient is the use of the Blade Element Momentum Theory (BEMT) including Prandtl's tip loss function (Ref. 10), and assuming the same airfoil behavior for the different radial stations. The main difficulty of this method is the determination of the sectional aerodynamic characteristics of the rotor's airfoil as a function of the angle of attack. For the specific curved plate airfoil used, a conservative value of C_{D0} is 0.1. In full-scale rotors the drag coefficient of the airfoils undergoes small variations with the angle of attack α, thus it is a good approximation to assume the drag coefficient $C_D(\alpha)$ constant and equal to C_{D0}. At MICOR's Re the variation in sectional drag coefficient with blade section angle of attack is not negligible anymore and it has to be considered. In general the sectional drag coefficient below stall can be approximated as

$$C_D(\alpha) = C_{D0} + d_1\alpha + d_2\alpha^2 \tag{15}$$

where d_1 and d_2 are empirically determined coefficients.

For the airfoil used and the Reynolds number range encountered by MICOR's rotor blades, no experimental data could be found. The BEMT model was used to obtain the airfoil's characteristics from the experimental rotor measurements and to determine the respective contributions of the induced and profile power to the total power required by the rotor.

Using power and thrust coefficients vs. collective pitch as target functions, sectional lift and drag characteristics were estimated from the experimental measurements with untwisted blades. Figure 10 compares the experimental and BEMT C_P vs. C_T for twisted and untwisted blades.

Sectional drag was approximated using Eq. (15) with $C_{D0} = 0.088$, $d_1 = 0$ and $d_2 = 2.28$. For the lowest thrust values the power coefficient is

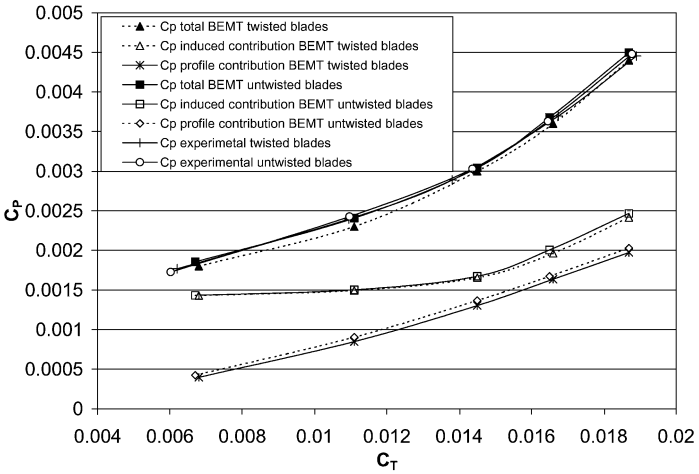

Fig. 10. C_T vs. C_P for single rotor, BEMT and experimental results.

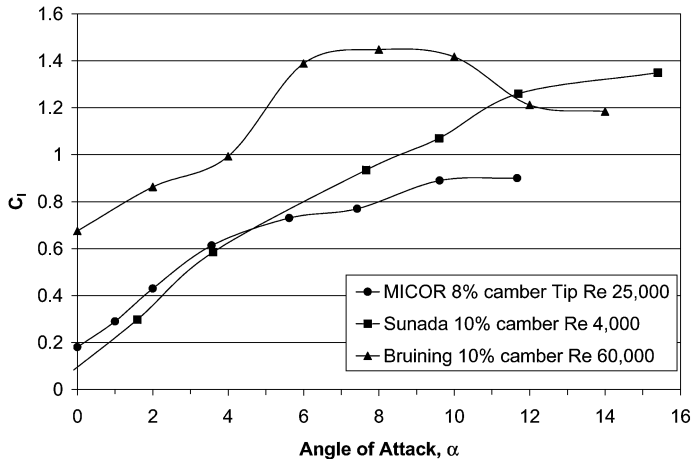

Fig. 11. Airfoil lift coefficient comparison.

underpredicted, since the quadratic function used is just an approximation of the real drag coefficient behavior. The resultant lift coefficients for the range of angles of attacks encountered by the rotor is shown in Fig. 11. The plot is typical for a low Re regime, highly nonlinear and with a low maximum lift coefficient. It is similar in shape to the measurements of Bruining (Ref. 12) for a thin 10% circular arc airfoil at Re of 60,000. Even for a collective pitch of 18 deg, the maximum angle of attack reached was not high enough to go beyond the maximum lift coefficient of the airfoil. The lift to drag ratio plot shown in Fig. 12 illustrates the relatively poor airfoil performance. The maximum lift to drag ratio reached is close to 6.8 at 5 deg angle of attack. The curve is relatively flat so the use of twist and taper is not as beneficial as in full-scale helicopters. Low lift to drag ratio might be a consequence of the presence of a laminar separation bubble in a large portion of the airfoil chord. If this is the case, one could potentially use a variety of passive techniques to trip the boundary layer and avoid the development of a laminar separation bubble.

In Fig. 8, BEMT *FM* vs. thrust coefficients for twisted and untwisted blades are compared. It can be observed that BEMT calculations predict an increase of around 5% in *FM* at the higher thrust coefficients for the twisted blades. The BEMT predictions of the induced power factor are presented in Fig. 13. As can be observed there is a reduction in the induced power factor by twisting the blades. In a full-scale helicopter, usually 30% of the power is consumed by the profile losses and 70% by the induced

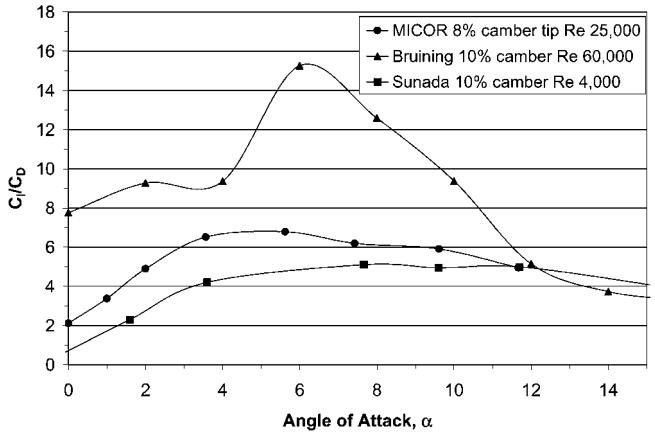

Fig. 12. Airfoil lift to drag ratio comparison.

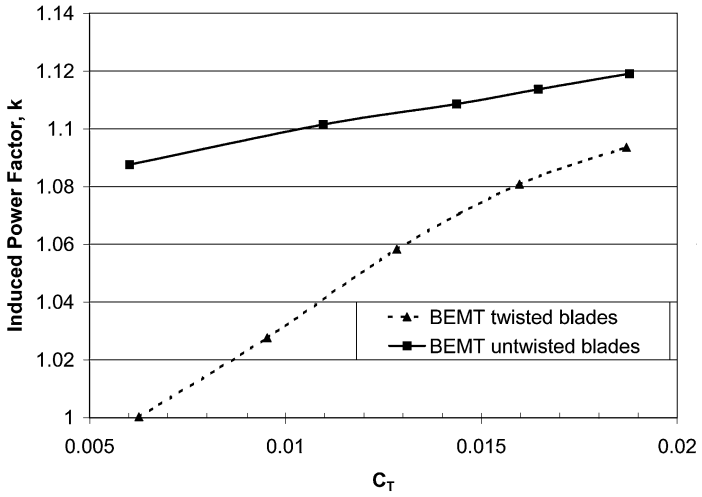

Fig. 13. Twisted blades: Experimental figure of merit vs. C_T.

losses. In Fig. 10 the power coefficients for twisted and untwisted blades with the induced and profile contributions are shown. At these low Re the profile drag has a larger influence over the total power required by the rotor. At high thrust coefficients the contribution of profile power goes up to 45%. This is the reason why the reduction in induced power does not have a large impact on the rotor performance. In fact, the increase in *FM* obtained when twisted blades are used is due to the simultaneous reduction of the profile and the induced power. The more uniform inflow distribution allows a larger portion of the rotor blades to work at a higher lift to drag ratio.

The difference between the experimental and the predicted increase in *FM* might be a consequence of experimental error especially in the measurement of the collective pitch of the rotor. It is possible that the centrifugal forces as well as the airfoil pitching moment modify the twist distribution elastically deforming the blades and the thin aluminum pins that support them. Even a small variation in the collective pitch or in the twist distribution has a significant influence on the performance of the rotor. Wind tunnel testing of the airfoils is required to determine the real airfoil characteristics at the working Re.

Future Work

In order to determine the flow separation mechanism acting on MICOR's blades, a flow visualization experiment will be performed. If the existence of a separation bubble is confirmed, the use of passive devices to trip the boundary layer will be investigated. Systematic testing of airfoils and blade planforms has already started in conjunction with a redesign and improvement of the hover test stand. The two proposed lateral control schemes are going to be implemented and evaluated in the flying prototype. In a parallel project, the introduction of high-frequency active pitching and flapping of the rotor blades is under investigation. Preliminary testing showed that the unsteady aerodynamic forces created by the induced blade pitching motion enhance the performance of rotors at low Reynolds number. A future MICOR prototype might make use of this approach to improve its performance. These presented results have revealed a number of issues that need to be investigated to understand the physics of hovering vehicles at low Re. Some of the important issues are:

1) Evaluation of different airfoil/blade geometries at low Reynolds number (Re $\leq$ 30,000).

2) Surface flow visualization of different rotor blade configurations to study laminar separation effects.

3) Wake flow visualizations to look into the topology of the flow and interaction between rotors.

4) Study of the effect of blade elasticity on rotor performance.

Summary and Conclusions

In summary, an initial design of a coaxial micro rotorcraft configuration has been developed and flight tested. The prototype design, called MICOR, weighs approximately 100 gm without a fuselage or lateral control fins. No length dimension of the vehicle exceeds 6 in. Preliminary flight testing of the MICOR vehicle using only onboard installed power demonstrated vertical ascent capability along with open loop differential yaw control. Flying times of three minutes were reached using three 430 mAh, 3-V $LiMnO_2$ batteries. Aerodynamic performance of the rotors was poor yielding a *FM* of 42% for a set of twisted blades. A BEMT model of the rotor was implemented, and airfoil characteristics were obtained. The model showed that profile drag accounts for 45% of the losses as opposed to 30% in full-scale helicopters. This fact considerably reduces the beneficial effects obtained when twisted blades are used. Much work is needed to make the MICOR a practical MAV. The highest priority is the improvement of the aerodynamic performance of the coaxial rotors and the reduction of the adverse effects of viscous drag at low Reynolds number.

Acknowledgments

The work was supported by the National Rotorcraft Technology Center, under contract no. NCC-2944, with Dr. Yung Yu serving as contract monitor. The authors would like thank Professor J. Gordon Leishman for his insightful suggestions and recommendations to improve the quality of our paper, and to Bernard LaFrance for his mechanical insights.

References

[1]Davis, W. R.,"Micro UAV," Proceedings of the 23rd Annual AUVSI Symposium, Orlando, FL, July 15–19, 1996, pp. 121–142.

[2]Hundley, R. O., and Gritton, E. C., "Future Technology-Driven Revolutions in Military Operations-Results of a Workshop," Document number DB-110-ARPA, RAND National Defense Research Institute, December, 1994, p. 105.

[3]Davis, Jr., W. R., Kosicki, B. B., Boroson, D. M., and Kostishack, D. F., "Micro Air Vehicles for Optical Surveillance," *The Lincoln Laboratory Journal*, Vol. 9, (2), 1998.

[4]Smith, J. O., Black, K. M., Kamangar, F. A., and Fitzer, J., "The University of Texas at Arlington Autonomous Aerial Vehicle—An

Overview," *Journal of Applied Intelligence*, Vol. 2, 1992, pp. 299–320.

[5]Stepniewski, W. Z., and Tarczynski, T., "Open Airscrew VTOL Concepts," NASA Contractor Report 177603, September 1992, p. 226.

[6]Woodley, B., Jones, H., Frew, E., LeMaster, E., and Rock, S., "A Contestant in the 1997 International Aerial Robotics Competition," Association for Unmanned Vehicle Systems International (AUVSI), 1997 Proceedings, Orlando, FL, July 1997. Aerospace Robotics Laboratory, Stanford University, (http://sun-valley.stanford.edu/papers/WoodleyJFLR:97.pdf).

[7]Zorpette, G., "Spying Saucer-Cypher," *Scientific American*, Vol. 276, June 1997, p. 40.

[8]Kroo, I., and Kruntz, P., "Development of the Mesicopter: A Miniature Autonomous Rotorcraft," Proceedings of the AHS Vertical Lift Aircraft Design Conference, San Francisco, CA, January 2000. CD-ROM Only.

[9]Stancil, C. M., "Electric Toroid Rotor Technology Development," Phase I study funded by NASA Institute for Advanced Concepts, April 30, 1999 (http://www.niac.usra.edu/studies/).

[10]Leishman, J. G., *Principles of Helicopters Aerodynamics*, Cambridge University Press, New York, 2000, pp. 69–70.

[11]Power Computing Solutions, "Electric Power System for High Altitude UAV Technology," NASA/CR-97-206337, 1997, p. 115.

[12]Bruining, A., "Aerodynamic Characteristics of a Curved Plate Airfoil Section at Reynolds Numbers 60,000 and 100,000 and Angles of Attack from −10 to +90 Degrees," Report Number VTH-LR-281, Dept. of Aerospace Engineering, Technische Hogeschool, Delft, Netherlands, May 1979.

[13]Sunada, S., "Comparison of Wings Characteristics at an Ultralow Reynolds Number," *Journal of Aircraft*, Vol. 39, March–April 2000.

[14]Coleman, C. P., "A Survey of Theoretical and Experimental Coaxial Rotor Aerodynamic Research," NASA Technical Paper 3675, March 1997.

[15]Langford, J. S., "The Daedalus Project: Summary of Lessons Learned," AIAA Aircraft Design, Systems and Operating Conference, Seattle, August 1989, Paper No. AIAA-89-2048, p. 12.

[16]Azuma, A., Okamoto, M., and Yasuda, K., "Aerodynamic Charateristics of Wings at Low Reynolds Number," *Fixed and Flapping Wing Aerodynamics for Micro Air Vehicle Applications, Progress in Astronautics and Aeronautics*, edited by Thomas J. Mueller, AIAA Reston, VA, Vol. 195, 2001, pp. 341–391.

[17]Sunada, S., Sakaguchi, A., and Kawachi, K., "Airfoil Section Characteristics at a Low Reynolds Number," *Journal of Fluids Engineering*, Vol. 119, March 1997, pp. 129–135.